Advances in Organic Photovoltaics and Methods for Effective Solar Cell Parameter Extraction

Graeme Williams*

Organic Optoelectronic Materials & Devices Laboratory

Electrical and Computer Engineering

University of Waterloo. Waterloo, ON Canada. N2L 3G1.

Correspondence should be addressed to g3willia@uwaterloo.ca

Abstract. Alternative and renewable sources of energy have been identified as key areas of research given our society's projected energy demands. Photovoltaics are the most likely candidate to meet the impending energy demands, with organic photovoltaics offering a uniquely cheap route to achieve energy sustainability. The development of organic photovoltaics (OPV) has been largely dictated by leaps of improvement in power conversion efficiency (PCE) values, owing to significant advances in materials properties and device architectures. These improvements have allowed for enhancement of PCE values from less than 0.1% with simple organic films to a current value of 8.13% for bulk heterojunction devices. This review will serve to examine the milestones of improvement in organic solar cells with a particular emphasis on device architecture and the associated device physics. Accompanying this discussion will be an overview of relevant device parameters and the current methods to reliably extract these values from experimental data.

1. Introduction.

With worldwide energy usage expected to nearly double by the year 2050 and worldwide oil reserves steadily depleting [1], research for alternative sources of energy has become paramount. Even with more advanced oil extraction techniques, it is expected that alternative, renewable sources of energy will be required by the end of the century. Given the huge amount of solar radiation impingent on the earth, photovoltaics have been identified as the most feasible candidate to meet the impending energy demands. Other approaches to provide the required energy are either insufficient – such as wind, geothermal, hydroelectric and tidal – or impractical – such as nuclear fission and fossil fuels in conjunction with carbon sequestration [1].

Efficient photovoltaics began with single crystal silicon, which is frequently termed first generation technology. These "p-i-n" solar cells generally achieve power conversion efficiency values of ~15%-20% commercially, with experimental cells developed in lab environments capable of 24-25% [2, 3]. Most recent advances are attributed to improvements in light in-coupling by optimizing the silicon surface geometry. With further improvements, the first generation of solar cells may reach their theoretical maximum efficiency of ~31%, defined as the Shockley-Quessier limit [4]. This limit was calculated by taking into consideration all insurmountable losses, especially due to energy losses from both low and high energy photons. High energy photons produce hot carriers well above the band edges of the semiconductor, which rapidly thermalize and thereby dissipate energy. In contrast, low energy photons below the bandgap of silicon (~1.1eV) cannot promote an electron from the valence band to the conduction band and are therefore lost as a source of energy.

From the above discussion, it is clear that single crystal silicon photovoltaics are technologically limited by their fixed bandgap energy. They are further economically limited by their high cost of production. In order to address these concerns, second and third generation photovoltaics have been developed. Third generation photovoltaics are focused on the use of nanocrystalline (quantum dot) materials that promise both reduced manufacturing costs and improved efficiency beyond the Shockley-Quessier limit. In order to achieve high efficiency values, third generation photovoltaics rely on hot carrier extraction and multiple generation effects; however, neither phenomena have yet been successfully applied to nanocrystalline solar cells in a practically relevant manner [5].

Second generation photovoltaics have lower efficiency values than first generation photovoltaics and rely on decreased manufacturing costs to gain an economic advantage. These are generally large area, thin film electronics and include vacuum-deposited amorphous or polycrystalline semiconductors as well as solution-deposited organic semiconductors. By removing the need for expensive physical or chemical vapour deposition, organic semiconductors gain a significant competitive advantage. The use of thin film, amorphous

organic films also allows for the possibility of flexible substrates in combination with high throughput reel-to-reel processing to further decrease costs. With most recent materials allowing for 8.13% power conversion efficiencies [6], organic solar cells are becoming a strong competitor in this particular generation of photovoltaics.

The structure of this review is as follows. Section 2 provides information on solar cell fundamentals and notable device parameters, which will be used to describe the performance of solar cells throughout this review. Section 3 serves to outline the history of organic photovoltaics, with the goal of providing insight into the fundamental device physics and the major challenges faced by this technology. Following this discussion, the device structure and materials used in the most current organic solar cells will be examined with a focus on device optimization and efficiency improvements. Section 4 will then focus on methods to reliably extract relevant solar cell parameters from the basic solar cell output data. Such discussions are especially relevant for the purpose of cross-comparisons among organic solar cells that can vary not only in structure, but also in materials composition.

2. **Background: Operation Principle and Notable Parameters.**

A solar cell is fundamentally composed of one or several light-absorbing layers placed between two electrodes, one of which must be transparent to allow for the passage of light. The active layer(s) absorb(s) light to generate free carriers, which are then collected at the electrodes. In an organic solar cell, the active layers are comprised of thin films of organic semiconductors, which may be formed through either solution-based methods for polymeric materials or through thermal evaporation for small-molecule materials.

This review article will focus on the polymeric, solution-deposited films, as these are most relevant toward the goal of economically viable solar cells. However, it should be noted that small molecule organic solar cells have also been successful in achieving high solar cell efficiencies [7, 8], and have gained strong notoriety for their use in photodetectors. Since small molecule films are vacuum deposited, multiple (>2) heterojunction devices have been shown to be feasible, allowing for strong gains in device quantum efficiency. The reader is strongly encouraged to examine reference [9] for a very thorough review by Forrest and coworkers on the subject of small molecule solar cells and photodiodes. A more recent review on the current status of small molecule organic solar cells is provided in [10].

In contrast to the conduction and valence bands with inorganic semiconductors, organic semiconductors are generally discussed in terms of the analogous quantities known as the lowest unoccupied molecular orbital (LUMO) and highest occupied molecular orbital (HOMO). Common organic solar cells make use of either plastic or glass substrates, with a tin-doped indium oxide (ITO) bottom electrode and a low work function metal top electrode (most

commonly calcium, magnesium or aluminum). This common configuration is shown in Figure 1 A) and B).

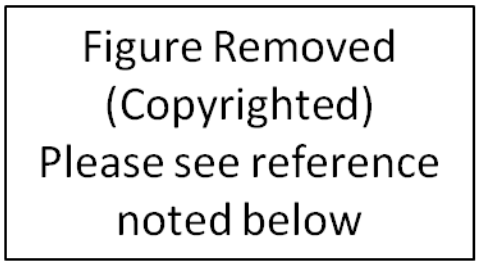

Figure 1 - A) Common structure of a simple, single-layer organic solar cell with B) associated energy diagrams of *separated* components. ϕ_{ITO}, ϕ_{Al}, χ, IP and E_g refer to the ITO work function, aluminum work function, and semiconductor electron affinity, ionization potential and bandgap respectively (Images adapted from ref [11]). C) Equivalent circuit model for an organic solar cell. The solar cell is fundamentally composed of a current source and a rectifying component, modelled as a diode. R_s and R_{sh} refer to series and shunt resistances respectively, which occur due to non-idealities within the solar cell.

In the simple illustration in Figure 1A) and B), a photon enters the device through the transparent electrode to generate an exciton within the organic semiconductor. The exciton is further broken down into an electron and a hole, which are collected at the aluminum and ITO electrodes respectively. It is important to note that these energy diagrams are only drawn for the isolated components and do not include band bending due to Fermi level alignment. The basis for preferential breaking of the exciton is discussed in greater detail in **Section 3**.

Given the above discussion, an organic solar cell under light exposure may be best understood as a current source. Due to the nature of exciton dissociation and carrier collection, as will be discussed in **Section 3**, the organic solar cell is also a rectifying device. Additional resistances, R_{series} and R_{shunt} may also be considered due to several non-idealities and inefficiencies in the device structure and operation. R_{series} occurs due to the contact resistances between the electrodes and the organic semiconductor, in addition to the resistances of the bulk semiconductor and the electrodes themselves. R_{shunt} is included due to leakage and recombination current within the device. A final equivalent circuit model of the organic solar cell is shown in Figure 1 C).

Simple comparisons among solar cells are usually made in terms of their power conversion efficiencies (PCE or η_{PCE}), which refer to the amount of useful electrical energy produced as a function of the input optical power. PCEs are typically reported in terms of a standard one-sun (100mW/cm^2), air mass 1.5 (AM1.5) exposure produced by a solar simulator. This spectrum is analogous to light impingent to the earth after it has traveled through the earth's atmosphere a distance of 1.5 atmosphere thicknesses. A number of other notable solar cell parameters include:

- I_{sc}: short circuit current – the solar cell current when the voltage across the solar cell is zero

- V_{oc}: open circuit voltage – the voltage across the solar cell when the solar cell current is zero
- FF: fill factor – the ratio of the 'actual' maximum output power to the 'possible' maximum power (where there are no losses due to R_s and R_{sh}). The fill factor is a measure of the solar cell's closeness to an ideal solar cell, defined as:

$$FF = \frac{V_m I_m}{V_{OC} I_{SC}} \quad (1)$$

, where V_m and I_m are the maximum voltage and current values respectively

- η_{EQE}: external quantum efficiency – the number of carriers collected per number of photons impingent on the solar cell at a given wavelength of interest. This quantity may also be referred to as the incident-photon-to-carrier efficiency, and is defined as:

$$IPCE = EQE = \eta_{QE} = \frac{hcI_{sc}(\lambda)}{e\lambda P(\lambda)} \quad (2)$$

, where h is Planck's constant, c is the speed of light, I_{sc} is the wavelength-dependent short circuit current, e is the charge of an electron, λ is the wavelength of light and P is the wavelength-dependent light intensity.

- η_{IQE}: internal quantum efficiency – the number of carriers collected per number of photons absorbed by the active organic semiconductor. This factor excludes optical losses due to reflection and transmission as well as losses due to absorption by non-active layers.

In terms of the above quantities, the PCE may be found as: $PCE = \frac{FFV_{OC}I_{SC}}{Input\ Optical\ Power\ (W)}$ (3)

3. Advances in Organic Photovoltaics

The early development of organic solar cells was driven by breakthroughs in device architecture with associated gains in device efficiencies. In a very brief period of time, organic solar cells evolved from simple monolayer structures placed between mismatched electrodes to more complex, phase-separated bulk heterojunctions. Later gains in device performance arrive primarily as a result of materials development, which relies heavily on the rapid prototyping of specially optimized polymers. Beyond these improvements in materials, gains in device efficiency and stability have arisen as a consequence of organic-electrode and organic-organic interface studies. The reasoning and logic behind the major organic solar cell breakthroughs along with the associated experimental gains are described herein.

3.1. Early Work in Device Architecture

3.1.1. Before Heterojunction Organic Solar Cells

The simplest form of an organic solar cell comprises a single homogenous organic semiconductor placed between a transparent conductive oxide (TCO) bottom electrode and a metallic top electrode. Some of the earliest work on this device architecture can be traced back to simple films of chlorophyll-a electrodeposited between two metal electrode in 1975 [12]. In both this work and much later work at Xerox in 1993 [13], it was shown that organic semiconductors have sufficient conductivity and hole carrier densities to form p-type Schottky barrier contacts with adjacent metal layers. In the latter work, the synthesized polymer poly(p-phenylene vinylene) (PPV) was used as the organic layer, although it is noted that polyacetylene and polythiophenes had been previously examined for similar purposes [11].

Riess et. al., Antoniadis et. al. and Marks et. al. further showed that favourable HOMO/LUMO bending at aluminum-PPV Schottky contacts could be used for photovoltaic applications in 1994 [14-16]. The energy diagram for this system is provided in Figure 2 A). Upon absorption of a photon, an exciton is formed in the PPV semiconductor. The exciton is dissociated into its constituent electron and hole due to the electric field at the Schottky contact. Electrons may be collected directly at the aluminum electrode, whereas holes must diffuse along the thickness to the semiconductor to be collected at the ITO electrode.

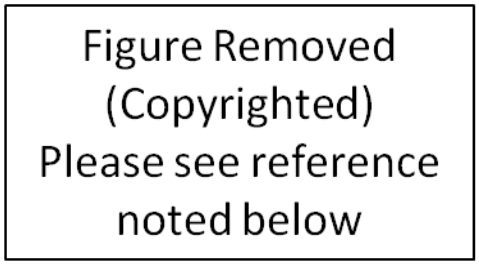

Figure 2 - A) Energy diagram for a simple PPV-Al Schottky solar cell. B) IV output characteristic for a representative PPV-Al Schottky solar cell. Note that the fill factor is rather poor (~0.2) and the current density is very low for solar cells made with this device structure. (Figures adapted from [14])

Each of these early studies identify similar open circuit voltages of ~1.2V, rather poor short circuit current values at 1-2 $\mu A/cm^2$ and power conversion efficiency values near ~0.1-1% for low light conditions [14, 15]. A representative IV output characteristic for this system is provided in Figure 2 B). Antoniadis et. al. note that further increasing the light source power results in smaller gains in photocurrent, thereby reducing the device efficiency. Although it is not directly reported, this effect is very likely due to a reduction in the device quantum efficiency as a consequence of bimolecular recombination. In this case, photogenerated electrons and holes interact and recombine either radiatively or non-radiatively. As such, an increase in photogenerated carrier density results in greater levels of recombination.

This simplistic structure is clearly limited in its capacity for photovoltaics, as proven by its underwhelming solar cell properties,. Excitons are dissociated primarily at the depletion layer formed at the Schottky contact. Since the exciton diffusion length is typically below 20nm

for organic materials [17], only a very small number of excitons generated very close to the Schottky contact contribute to harvestable carriers and photocurrent. The active organic layer must be thick, however, or it will not efficiently absorb light due to significant transmittance losses.

3.2. Planar Heterojunction Organic Solar Cells

In order to address the poor device behaviour and losses associated with single layer organic solar cells, researchers sought device structures that encouraged exciton dissociation. Such an approach had already been applied with thermally evaporated small molecules since 1986 by Tang from Kodak [18]. In this work, Tang used a copper pthalocyanine (CuPC)-perylene tetracarboxylic planar junction to achieve power conversion efficiencies of 0.95% with fill factors as high as 0.65.

In the early work by Tang, it was shown that the offset in HOMO/LUMO of the two organic semiconductors allowed the heterojunction to act as an efficient interface for exciton dissociation. The material with higher electron affinity is denoted as the acceptor, whereas the material with lower electron affinity is denoted as the donor. Under exposure to light, a photogenerated exciton formed on a donor molecule may diffuse to the heterojunction, where its electron can rapidly transfer to an acceptor molecule. This transfer is favourable as long as the LUMO offset between the donor and acceptor is larger than the Coulombic stabilization energy of the exciton. More recent work has also shown probable dipole formation at the donor-acceptor interface, which further helps to separate electron-hole pairs and also hinders geminate recombination [19].

Upon exciton dissociation, the free carriers may then diffuse to their corresponding electrodes where they are collected to generate photocurrent. This process is shown in Figure 3. In contrast to the single layer device, which must support bipolar transport, a heterojunction device allows for electron transport along the high electron affinity material and hole transport along the low ionization potential material. This scheme significantly reduces bimolecular recombination and thereby increases photocurrent. As an additional benefit, since the heterojunction is present in the bulk of the film, the number of excitons within diffusion length of the junction increases substantially compared to the simple Schottky solar cell.

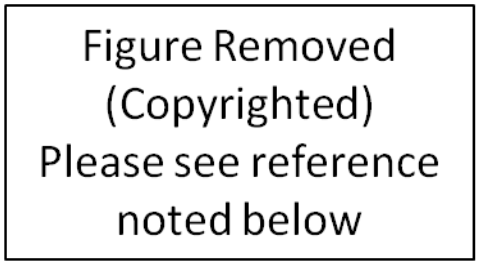

Figure 3 - Energy diagram of the HOMO/LUMO offset for a planar heterojunction organic solar cell. The energy levels are drawn for individual, separate components to show the general device behaviour. Contact between the organic layers and the electrodes may lead to some HOMO/LUMO bending, which has not been shown here. (Figure adapted from ref [11]).

The difficulty of incorporating a planar heterojunction in polymeric solar cells arises from solution-coating a top polymer layer without re-dissolving the underlying polymer layer. Methods to accomplish this task generally include making use of orthogonal solvents, which dissolve one polymer but not the other, or through the use of polymer precursors, where an insoluble polymer film is formed directly on the substrate. Later work in 1999 and 2000 showed these approaches to be feasible [20, 21], although by then much of the research had shifted to bulk heterojunction solar cells, which are described further in **Section 3.3**.

As a consequence, much of the early work in planar heterojunctions involved purely small molecule films, as discussed in Forrest and coworkers' review [9]. Other groups combined polymers and small molecules into solar cells by spincoating a bottom polymeric layer and subliming a strong acceptor layer on top, including perylene derivatives [22, 23] and fullerene (C_{60}) [24-28]. While these devices are inherently expensive, as they require a multi-step fabrication process involving both solution- and vacuum-deposition of organic materials, they served as an important milestone for efficiency. These devices also provided insight into organic solar cell device behaviour and architecture and, as such, are described briefly below.

The use of C_{60} in organic photovoltaics arose as a consequence of their proven quenching of organic excited states. In this early work, Sariciftci et. al. prepared thin films of poly[2-methoxy,5-(2'-ethyl-hexyloxy)-p-phenylene vinylene] (MEH-PPV) sensitized with small concentrations of C_{60} [29]. The researchers witnessed near complete loss of photoluminescence and a decrease in luminescence decay time in the composite compared to a pure MEH-PPV film, indicative of fast (~ps) electron transfer from MEH-PPV to C_{60}. The absence of new absorption spectral features further showed that no such transfer occurs at the ground state. This work was simultaneously completed by Morita et. al. for a different polymer, showing that the significant quenching of photoluminescence intensity could be achieved at C_{60} concentrations as low as 1% [30]. Later work by Lee et. al. demonstrated this effect for a different polymer, and also described an associated enhancement in photoconductivity for the composite polymer:C_{60} films. This gain in photoconductivity was attributed to extended free carrier lifetime arising from decreased radiative recombination [31].

Sariciftci et. al. were the first to examine polymer-C_{60} heterojunctions in 1993 with an ITO/MEH-PPV/C_{60}/Au structure [27, 28]. This device showed some improvement in fill factor to 0.48, but it exhibited poor power conversion efficiencies of ~0.04% when exposed to light with 1mW/cm^2 intensity. The device also exhibited significantly lower dark current than its single-layer predecessor and showed a linear current dependence on light intensity. These results prove that the device structure is successful in inhibiting bipolar transport across individual layers, thus limiting bimolecular recombination. These were results were confirmed by Morita et. al. with a thiophene-based polymer-C_{60} heterojunction showing good device rectification and measurable photocurrent [25].

These simple planar heterojunctions showed very modest improvements in external quantum efficiency with optimization of device fabrication [23, 24]. The underwhelming device performances highlight a fundamental problem with the planar heterojunction structure: most of the photogenerated excitons are not within their diffusion length of the heterojunction. This fact was emphasized in a study by Roman et. al., who calculated the point of maximum optical electric field of monochromatic light within a simple polymer-C_{60} planar heterojunction [26]. This research showed that by designing the device such that the maximum electric field was centred on the heterojunction, it was feasible to substantially increase the quantum efficiency of the device. This improvement is due to the increase in the number of excitons generated very near heterojunction, where free carriers may be generated.

As a point of interest, in 1998, Friend and coworkers showed some success with planar heterojunction films composed of a polythiophene donor and a cyano-based derivative of MEH-PPV as an acceptor [32]. In contrast to the above work, the acceptor film was doped with ~5% of the donor species and, similarly, the donor film was doped with ~5% of the acceptor species. This work was further unique in that the donor/acceptor films were formed on two different substrates and a lamination method was used to couple the device together. This fabrication approach is incredibly attractive, as the metal-coated substrates can be pre-prepared very cheaply and the active layers only require simple solution-based processing. Using this approach, the authors were able to achieve more reasonable PCE values of 1.9% under 77mW/cm^2, AM1.5 exposure conditions. This notion of laminate-processing of solar cells was revisited much later in 2008 by Yang and coworkers [33].

3.3. Bulk Heterojunction Organic Solar Cells

The bulk heterojunction concept was introduced as an answer to the poor efficiencies that arise due to excitons being generated too far from the planar heterojunction. In a bulk heterojunction, the donor and acceptor species are blended together in a common solvent and deposited simultaneously, as shown in Figure 4 A). By blending the two species together, one may ensure that photogenerated excitons will always be within their diffusion length of a heterojunction. As such, one can minimize recombination of the photogenerated excitons. It is

also worth noting that, while both electrodes are in direct contact with both the donor and acceptor materials in a bulk heterojunction, electrode work function mismatch allows for a sufficiently large internal electric field to collect separated carriers at the proper electrodes. This is shown in the simplified energy diagram in Figure 4 B), which illustrates a bulk heterojunction device under short-circuit conditions.

If the blend is defined properly, both the donor and acceptor may percolate across the electrodes, allowing for a blended film that exhibits bicontinuous phases. The interpenetrating network allows for efficient free carrier motion across the active layer of the device, as the holes may remain in the donor phase and the electrons may remain in the acceptor phase. This bicontinuous distribution of materials occurs naturally with polymer/polymer and polymer/small molecule mixtures deposited from solution due to the low entropy of mixing of macromolecules. By evaporating the solvent during deposition in a controlled manner, it is feasible to 'freeze' the device in this bicontinuous phase configuration.

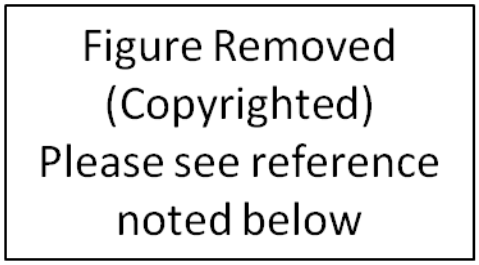

Figure 4 - A) Illustration of a bulk heterojunction placed between ITO and Al electrodes. Note that the donor (red) and acceptor species (blue) are well dispersed throughout the active layer and show discrete phases. B) Simplified energy diagram of the same. Interfacial band bending and associated effects have been ignored for simplicity. Also note that the LUMO and HOMO levels are shown as continuous across the entire film, which is not necessarily true unless the film shows ideal mixing. (Images adapted from ref [11] and ref [34]).

Following the success of C_{60} when used as an electron accepting species, Yu et. al. formed simple ITO/MEH-PPV:C_{60}/Ca bulk heterojunction devices in 1994 for use as photodetectors [35]. The inclusion of ~10% C_{60} by weight improved the photocurrent response of the photodiode by nearly an order of magnitude. Unfortunately, the weight ratio of C_{60} in the film is fundamentally limited by the poor solubility of C_{60}. It is therefore unrealistic to assume proper C_{60} phase distribution and separation within the organic film. In order to enhance the solubility of C_{60}, Hummelen et. al. examined fulleroid and methanofullerene derivatives that offer enhanced solubility due to bulky side-groups which inhibit fullerene aggregation [36]. In this work, the researchers developed phenyl-C61-butyric acid methyl ester (PCBM), which shows high solubility in most common organic solvents.

In 1995, Yu et. al. continued their earlier work from [35], replacing C_{60} with PCBM to form bulk heterojunction devices with higher acceptor concentrations [37]. The authors successfully increased the amount of PCBM to a weight ratio of 4:1 PCBM:MEH-PPV, such that roughly every repeat unit on the polymer would have a corresponding fullerene acceptor.

Devices made using an ITO/MEH-PPV:PCBM/Ca structure were capable of achieving I_{sc}, V_{oc}, peak EQE and PCE values of 2mA/cm^2, 0.82V, 29% and 2.9% respectively when exposed to 20mW/cm^2 monochromatic (430nm) light. The power conversion efficiency reported in [37] is a substantial improvement over previous single layer organic solar cells and serves as a milestone in organic photovoltaics. These devices also showed a nearly linear dependence of photocurrent on light intensity, further emphasizing that the bulk heterojunction structure inhibits bimolecular recombination.

In the same year, both Yu et. al. and Halls et. al. developed bulk heterojunction solar cells based on mixed donor/acceptor polymers [38, 39]. In both cases, the researchers made use of MEH-PPV as the donor and CN-PPV as the acceptor since CN-PPV has a higher electron affinity and a lower ionization potential. Fast electron transfer from MEH-PPV to CN-PPV was first shown via steady state photoluminescence measurements, where the photoluminescence intensity dropped considerably for mixing ratios between 1:4 and 4:1 CN-PPV:MEH:PPV by weight. Both groups obtained similar peak EQE values of 5-6%, with Yu et. al. reporting PCE values on the order of 0.9% when illuminated under low intensity, monochromatic light.

In both [37, 38], Yu et. al. noted that the open circuit voltage decreased from ~1.3-1.6V for a single layer MEH-PPV device to ~1V and ~0.8V for the MEH-PPV:CN-PPV and MEH-PPV:PCBM bulk heterojunction devices respectively. The authors note that the same reduction in open circuit voltage occurs with pure, single layer CN-PPV devices. While the origin of this variation has been subject to some debate, recent results and discussions from Crispin et. al. and Braun et. al. strongly suggest this work function lowering is due to a Fermi level pinning effect at the electrode-organic interface [40, 41].

In brief, one may describe single layer MEH-PPV solar cell devices as thin-film diodes based on a fully depleted Schottky diode scheme [38]. This conclusion has been made from two significant pieces of information:

- V_{oc} is dictated only by the work function difference between the electrodes
- Single layer devices exhibit constant capacitance across the device for voltages below V_{oc}, implying that the polymeric layer is already fully depleted

This simple MEH-PPV-based device behaviour arises because the HOMO is lower than the Fermi level of ITO and the LUMO is higher than the Fermi level of Ca. However, since CN-PPV and PCBM have electron affinities greater than the work function of Ca, solar cells making use of these materials show an altered (lowered) open circuit voltage due to Fermi level pinning. Additional lowering of the V_{oc} may be due to device non-idealities, relating to poor fill factors caused by high series resistances and low shunt resistances. The topic of open circuit voltage is discussed in greater detail in **Section 3.4.2**.

3.4. Enhancement and Optimization of Modern Organic Solar Cells

Much of the groundwork for modern organic photovoltaics was set with the development of the bulk heterojunction and with the realization of PCBM as an acceptor material. Following the initial successes described above, there was a huge surge of research interest in organic photovoltaics. The remainder of this review will therefore focus on the most prominent and successful class of organic solar cells, which were based off of the nascent results described above: fullerene/PCBM-based bulk heterojunctions.

As a point of note, very interesting work has also been completed on the development of block copolymers, where a single polymer chain comprises of both donor and acceptor groups [42-45]. In such a system, the differing blocks tend to phase separate, which is ideal for application in bulk heterojunctions. Unfortunately, these cells generally exhibit poorer performance than simple mixed-polymer systems, with very recent work in 2009 only showing 0.49% PCE [46]. Readers interested in these developments are referred to [42], where Sun discusses the fundamental requirements for acceptor-donor block copolymers.

3.4.1. Improvement in Device Efficiencies through Advances with the Donor Material

Bulk Heterojunction Solar Cells with PPV-Based Donor Materials

In the early work on organic photovoltaics, researchers made use of PPV and PPV-derivative polymers as the primary absorbing and donor species in heterojunction cells [27, 28, 37]. In 2001, Shaheen et. al. developed bulk heterojunctions of poly[2-methyl,5-(3*,7** dimethyloctyloxy)]-p-phenylene vinylene) (MDMO-PPV) with PCBM to produce solar cells with 2.5% PCE, the highest reported efficiencies for polymeric solar cells at the time [47]. Much of the improvement witnessed in this particular experiment can be attributed to two experimental considerations:

- The use of chlorobenzene (CB) instead of toluene as a solvent for spincoating allowed for much smoother films, owing to better polymer mixing and polymer phase distribution.
- The high concentration of PCBM in the composite allowed for a larger number of PCBM percolation pathways and also granted better mobility for both electrons and holes within the film.

The first experimental consideration highlights the importance of film morphology for bulk heterojunctions, which remains a concern in all bulk heterojunction organic photovoltaics regardless of the chosen donor species. In their 2007 review, Günes et. al. listed a number of factors that may affect the characteristics of the solution-deposited film, including: the solvent, the processing temperature, the ratio of the donor to acceptor, the concentration and the chemical structure of the chemical species [48]. Beyond these factors, the method of depositing the film (spincasting, dropcasting, doctor blading, etc.), the cleanliness of the

deposition environment (typically a nitrogen glovebox) and the time between solution preparation and deposition can all have significant effects on film quality and morphology.

The second experimental consideration further stresses the importance of film morphology, but also notes the anomalous increase in hole mobility when MDMO-PPV is incorporated into a blend structure with PCBM. Melzer et. al. found that the hole mobility in a 20:80% MDMO-PPV:PCBM film was only an order of magnitude lower than the electron mobility in a pure PCBM film [49, 50]. This is in contrast to the pure MDMO-PPV film, where the hole mobility is four orders of magnitude smaller than the pure PCBM film electron mobility. This phenomenon is counterintuitive; increasing the PCBM concentration dilutes the MDMO-PPV concentration and should decrease the number of conductive pathways for hole transport. While the cause of this phenomenon has not yet been identified, it has been suggested that the improvements arise from a change in the configuration of the PPV-based polymers, which allows for better $\pi-\pi$ stacking and therefore grants higher carrier mobility.

Despite the impressive initial 2.5% PCE shown by Shaheen et. al. [47], further improvement in PPV-PCBM-based bulk heterojunctions only allowed for modest increases in PCE values of 3 to 3.3% [51-53]. Even with the anomalous increase in hole mobility noted above, the mobility and associated conductivity of PPV polymers are still quite low. Furthermore, the wide bandgap of PPV polymers prohibits the absorption of low energy photons and thereby restricts the maximum photocurrent. For this reason, researchers began examining small bandgap polymers and polymers with higher hole mobilities. As a point of note, hole mobility is typically inversely related to ionization potential for organic materials. Given similar bandgap energies and film forming capabilities, a high hole mobility material should then exhibit a larger HOMO/LUMO offset with PCBM, as shown with poly-3(hexylthiophene) (P3HT) in Figure 5 A).

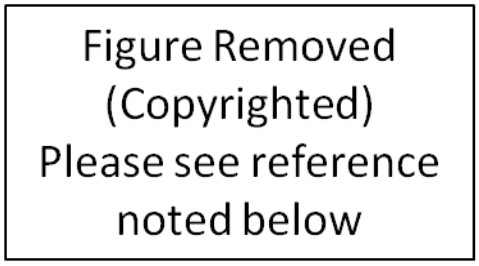

Figure 5 - A) Illustration of the difference in HOMO/LUMO and bandgap for P3HT vs. MEH-PPV donor polymers when used in bulk heterojunction organic solar cells with PCBM. (Figure adapted from ref [54]). B) EQE curves at two active layer thicknesses for the preliminary P3HT:PCBM devices discussed in ref [55]. (Figure adapted from ref [55]).

Bulk Heterojunction Solar Cells with P3HT Donor Materials

For much of the past decade, P3HT:PCBM bulk heterojunctions have been the focus for organic solar cells. The shift to P3HT as a donor species began with promising results in 2002 from Schilinsky et. al., who showed that ITO/PEDOT:PSS/P3HT:PCBM/Ca devices could achieve

very high EQE values, as shown in Figure 5 B) [55]. In this work, they also showed an increase in short circuit current with increasing temperature, as well as the capacity for the system to achieve an IQE near 100% at the peak absorption wavelength of ~550nm.

Post-processing techniques later allowed for increases in P3HT:PCBM-based PCE values to 3.5% [56]. In this work, the researchers heated the as-fabricated device (with the same structure as [55], except with an LiF/Al top electrode) above the glass transition temperature of P3HT while simultaneously applying an electrical bias to the device. Increasing the temperature of the polymer beyond its glass transition temperature allowed the P3HT:PCBM polymer mixture to reorganize itself and phase separate more effectively than in the initial casting of the film. The authors suggest that the electrical bias applied to the film further encouraged the polymer to orient itself in such a manner to allow for efficient charge transport.

Significant work has been dedicated to the optimization of process conditions for P3HT:PCBM bulk heterojunctions in much the same manner as was discussed for PPV:PCBM solar cells. The reader is encouraged to examine [57] and [58] by Brabec and coworkers for tabulated data on this topic. In general, researchers have sought to optimize the percolation, structure and orientation of both the donor and acceptor materials in the film through variations in materials properties, deposition conditions and post-processing treatments [59-74]. A detailed analysis of the major conclusions regarding optimization of P3HT within the P3HT:PCBM active layer in bulk heterojunction devices is provided below. While these optimizations have been made for P3HT:PCBM heterojunctions, much of these considerations can and should be extended to future donor materials. This sum of knowledge has allowed for reasonable levels of reproducibility in device fabrication among different groups, with reported PCE values on the order of 4-5% [63, 65, 66, 71, 75].

The highest efficiencies for P3HT:PCBM bulk heterojunction solar cells are obtained at active layer compositions of 0.8-1:1 P3HT:PCBM by weight [59, 61, 63, 66]. At these concentrations, the P3HT:PCBM film exhibits balanced electron and hole transport and is less susceptible to space-charge limited carrier transport. Furthermore, this balanced concentration allows for percolation of both PCBM and P3HT within the bulk heterojunction and across the length of the device. This is a much lower 'ideal' PCBM concentration compared to PPV:PCBM-based solar cells. One reason for this variation is that P3HT films have higher 'pure' hole mobilities and P3HT:PCBM films therefore do not benefit from the same anomalous hole mobility improvements as described above for PPV:PCBM-based devices. As an additional factor, at very high PCBM concentrations, thermal annealing of the P3HT:PCBM film leads to the formation of large PCBM crystallites that cause film cracking and drastically increase the organic-metal electrode contact resistance [59, 67].

Following the results from [56], thermal annealing of P3HT:PCBM bulk heterojunction devices was found to result in improved EQE, short circuit current, fill factor and device PCE

values [62-66, 69], as shown in Figure 6 A). This has been attributed to better phase separation of the polymers and due to the formation of both PCBM nanocrystallites and larger P3HT crystallites, allowing for high carrier mobilities [65, 67, 69, 74]. For the same reasons, slow drying or "solvent annealing" of the P3HT:PCBM film allows for higher device efficiencies [61, 63, 72, 73], as shown in Figure 6 B). To prove this effect, Li et. al. showed that the optical absorption of a thick, slowly dried film was the same pre- and post-anneal. In contrast, a quickly dried film developed the characteristic crystalline P3HT peaks only after annealing, indicating poor initial film morphology [63], as shown in Figure 6 C). Furthermore, the slowly dried sample exhibits a strongly red-shifted absorption curve, which implies a higher degree of molecular π-π interaction (granting higher hole mobility) due to structural ordering. The solvent annealing approach may be pertinent for very low temperature manufacturing processes for highly flexible substrates or for newly developed donor polymers that are unstable at elevated temperatures.

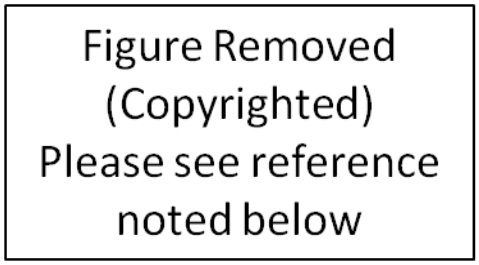

Figure 6 - A) IV output characteristics for P3HT:PCBM bulk heterojunction solar cells that have undergone thermal annealing. Devices 1-4 correspond to devices with 0min, 10min, 20min and 30min treatment at 110^{o}C, performed prior to top electrode deposition. The active layer in all devices was 210nm and the film was dried slowly for 20 minutes prior to thermal annealing. B) IV output characteristics for P3HT:PCBM bulk heterojunction solar cells with different active layer drying times. Devices 5-8 correspond to drying times of 20 minutes, 3minutes, 40 seconds and 20 seconds respectively. C) Absorption of P3HT:PCBM active layers with varying dry times, as cast and annealed. (Figures adapted from ref [63])

Some additional useful knowledge gleaned from the numerous P3HT:PCBM bulk heterojunction solar cell optimization experiments include:

- Annealing the P3HT:PCBM film after top electrode deposition (on a completed device) provides better efficiencies than annealing the sample prior to top electrode deposition [64, 65]. This has been attributed to enhanced interfacial chemical bonding and potential metal diffusion during the annealing process, which may allow for decreased interfacial carrier recombination and a larger contact area to reduce contact resistance.
- Increasing the device temperature during testing increases the short circuit current. The authors attribute this due to reduced trap-induced carrier recombination. In this regard, the thermal energy k_BT is greater than the energy of the trap state, so rapid de-trapping occurs and trap-induced recombination is minimized [60].
- Thicker P3HT:PCBM films minimize pinholes and cracking, thereby reducing leakage current and increasing shunt resistance [63].

- P3HT:PCBM films spun from dichlorobenzene (DCB) lead to devices with better as-spun efficiencies; however, these films generally require higher temperature annealing [62]. This variation is due to the lower volatility of DCB compared to CB, which leads to a longer film drying time and thereby increases the as-spun efficiencies for the same reasons discussed above and noted in [63].
- The addition of a non-solvent can be used to control P3HT aggregation in solution and therefore control the formation of P3HT crystallites within a cast film [75]. This method has been successfully applied to produce as-cast samples with ~4% power conversion efficiency. Similar to solvent annealing, the absence of a heat-treatment in this non-solvent approach may be useful for very low temperature manufacturing processes and for future temperature-sensitive polymers.

Schilinsky et. al. also found that a large P3HT molecular weight (MW), greater than 10 kDa, is required for high efficiency P3HT:PCBM bulk heterojunction solar cells [68]. The authors note that MW is directly related to intermolecular π-π interactions and to the formation of P3HT crystallites, as observed by the absence of the characteristic crystalline P3HT absorption peaks in small MW P3HT samples. This was further evidenced by the fact that high MW P3HT samples generally yield films with higher measured hole mobilities.

It was later found that the annealing treatment must be fine-tuned to different MW polymers, with larger MW P3HT requiring higher anneal temperatures and longer anneal times [70]. This variation is related to the stronger degree of aggregation for large MW P3HT polymer chains, which hinders phase separation and slows diffusion of PCBM throughout the film. Unfortunately, more intense annealing of the P3HT:PCBM film tends to induce the formation of large PCBM crystallites, which, as noted above, degrade device performance and cause reliability issues due to film cracking. In both [70] and later work in [74], an ideal composition of P3HT was found to include a mixture of both large and small MW P3HT, where the small MW P3HT forms an amorphous matrix around large MW P3HT crystallites. In this manner, the large MW P3HT is used for its enhanced electrical properties and the small MW P3HT is used to improve processability of the material. As such, high efficiency devices may most feasibly be formed by high MW polymers with high polydispersity.

The degree of regioregularity (RR) of P3HT, which is defined as the percentage of head-to-tail versus head-to-head or tail-to-tail monomers within the polymer, was also found to have a significant effect on the P3HT:PCBM bulk heterojunction solar cell properties. Highly RR P3HT is necessary for P3HT crystallite formation, and is therefore required for high hole mobility in the P3HT phase of a P3HT:PCBM film [71]. This follows from the fact that high RR allows for stronger polymer chain/intermolecular interactions through π-π stacking and therefore decreases the intermolecular distances of neighbouring chains. As a consequence, the degree of RR is closely associated with the solar cell photocurrent, fill factor and PCE. This effect was noted by Kim et.al., with a greater than two-times increase in photocurrent, EQE and PCE for

P3HT:PCBM bulk heterojunction solar cells made with 95.2% RR P3HT over the same cells made with 90.7% RR P3HT [71].

Bulk Heterojunction Solar Cells with High V_{OC} and High I_{SC} Polymers

The two major factors that drive the maximum efficiency of any solar cell are the short circuit current and the open circuit voltage, which may be tailored by altering the donor and acceptor materials in a bulk heterojunction solar cell. The reader is encouraged to examine a very thorough review by Bundgaard and Krebs [54] for more details on the polymer synthesis for high performance solar cells. This area of research is critical for organic photovoltaics, but given the scope of the current review, it is only briefly discussed here. The open circuit voltage for P3HT:PCBM bulk heterojunction solar cells is generally on the order of ~0.5-0.6V, which is less than one third of the thermodynamic limit imposed by the bandgap of P3HT (~1.9eV). In order to improve upon the low open circuit voltage, researchers sought to develop materials with deeper HOMO energy levels (equivalently, larger ionization potentials). The open circuit voltage is effectively set by the HOMO of the donor and the LUMO of the acceptor, as discussed in greater detail in **Section 3.4.2**.

To this end, researchers have studied both polyfluorenes [76-80] and poly(2,7)carbazoles [81-83] with reasonable levels of success. Polyfluorene-PCBM bulk heterojunction solar cells were shown to be capable of ~1V open circuit voltage, but exhibited relatively poor photocurrents (<10mA/cm^2) and low fill factors. Carbazole-based materials benefit from the fact that they are fully aromatic and are generally more stable than polyfluorenes [81]. These polymers have achieved bulk heterojunction open circuit voltages of ~0.9V with reasonable fill factors (>0.6), but they also exhibit low (~10 mA/cm^2) photocurrents. In a recent study, it was shown that an optimized polycarbazole-PCBM bulk heterojunction solar cell could achieve 6.1% PCE and near-100% IQE across a large portion of the visible spectrum [83]. The authors note that by decreasing the bandgap of the polycarbazole derivative, it should be feasible to maintain this high level of IQE in the red to infrared spectrum, allowing for potential PCE values of 10-15%.

The most recent gains in organic solar cell efficiencies are attributed to polymers that address the issue of low photocurrent while maintaining a reasonably high open circuit voltage. This restriction strongly complicates the design of the donor polymer. These polymers must have a deep HOMO for large open circuit voltage and polymer stability, and a small bandgap for high short circuit current. However, the HOMO must not be too deep or the hole mobility will be hindered. The donor polymer must also have a LUMO offset to the LUMO of PCBM to allow for efficient exciton dissociation. This offset must not be too large or the difference will be lost as thermal energy. As a final point, these polymers must also be stable and easily processable, which typically requires the use of bulky side-chains. However, these side chains must not negatively impact the π-π stacking of the polymer or the mobility will be severely compromised.

Poly(thienothiophene-benzodithiophene) (PTB) polymers appear to address many of these design constraints [84-87]. The PTB polymers are typically referred to as PTBx, where x is a number referring to a particular incarnation of the polymer, as detailed in [84]. As a point of note, when examining smaller bandgap materials, researchers usually employ $PC_{71}BM$, which uses a 70-carbon fullerene instead of the traditional 60-carbon "buckyball." This form of fullerene absorbs more strongly in the ~300nm-500nm wavelengths to allow for efficient solar cell absorption across the entire visible spectrum. PTB7 has very recently shown to allow for a bulk heterojunction PCE of 7.4% [86], which is the highest efficiency reported in research literature to date. This optimized PTB7 structure attained very impressive short circuit current, open circuit voltage and fill factor values of 14.5mA/cm^2, 0.74V and 0.69 respectively. The structure of Solarmer's record 8.13% efficiency organic solar cell is not available [6], but given that [84-86] were published by Solarmer researchers, it is likely that this solar cell also makes use of a donor polymer within the PTB family.

3.4.2. Origin of Open Circuit Voltage and Interfacial Optimization

While the basic operation of a bulk heterojunction device has been elucidated for some time, the origin of the open circuit voltage has remained subject to some debate. The open circuit voltage is a function of a large number of device and experimental parameters, including temperature, photoconductivity/resistance across the active layers, electrode resistance, dark current, donor/acceptor mixing and carrier recombination [88]. As noted above, early reports in organic photovoltaics showed the open circuit voltage to be driven primarily by the work function difference of the contact electrodes [38]; however, later work on P3HT:PCBM bulk heterojunctions indicated a HOMO/LUMO dependence on the constituent materials [89, 90]. This discrepancy was attributed to Fermi level pinning, such that the open circuit voltage is directly controlled by the LUMO of the acceptor [89] and the HOMO of the donor [90].

As a refinement to this definition, Cravino claims that the open circuit voltage is better defined by the difference between the LUMO of the acceptor and the single occupied molecular orbital (SOMO). This definition accounts for a 0.3V to 0.4V reduction from the ideal open circuit voltage commonly observed in organic solar cells [88]. In this manner, the energy offset due to the formation of a polaron in the organic material is taken into consideration. Rand et. al. offered a similar justification for the reduction in open circuit voltage, noting losses due to the dissociation of the geminate-polaron pair and subsequent losses in the relaxation of the electron and hole into their polaronic states [91].

Crispin et. al. further examined the impact of the polaronic states at the organic-electrode interface [40], and Braun et. al. later proposed the integer charge-transfer model to account for the impact of these states in the calculation of the open circuit voltage [41]. This model applies to weakly interacting interfaces, such as those formed between organic materials and metals/conductive oxides as well as those formed between two organic materials. In these

cases, a surface oxide or residual hydrocarbon layer prevent direct electron transfer across the interface, but still allow for electron transfer via tunnelling, leading to the formation of interfacial polarons and bipolarons within the organic material. The authors note that the interfacial polarons exhibit stronger binding energies than polarons formed in the bulk of the organic layer, which they attribute to image potential interaction between the polarons and the conducting surface, as shown in Figure 7 C). These surface states are denoted as positive (E_{ICT+}) and negative (E_{ICT-}) integer charge-transfer states.

One may then note three regimes for the organic-electrode interface formation depending on the work function of the electrode (ϕ_{el}):

- a) $\phi_{el} > E_{ICT+}$: Energetically-favourable tunnelling from the positive charge-transfer state to the electrode results in the formation of a dipole between the negatively-charged electrode surface and the positively charged organic surface polarons. This dipole down-shifts the vacuum level until the Fermi level of the electrode is aligned or pinned to the positive charge-transfer state, as shown in Figure 7 A) i). This is the case for P3HT and ITO as well as P3HT and PEDOT:PSS/ITO, and results in the experimentally observed open circuit voltage dependence on the HOMO of P3HT [90].
- b) $E_{ICT-} < \phi_{el} < E_{ICT+}$: Neither tunnelling from the E_{ICT+} state to the metal nor tunnelling from the metal to the E_{ICT-} are energetically favourable. No Fermi level pinning of the electrode occurs, as shown in Figure 7 A) ii). This simple regime corresponds to the early single layer MEH-PPV solar cells [38], where the open circuit voltage is determined simply by the work function difference of the electrodes.
- c) $\phi_{el} < E_{ICT+}$: Energetically-favourable tunnelling from the electrode to the negative charge-transfer state results in the formation of a dipole between the positively-charged electrode surface and the negatively charged organic surface polarons or bipolarons. This dipole up-shifts the vacuum level until the Fermi level of the electrode is aligned or pinned to the negative charge-transfer state, as shown in Figure 7 A) iii). This is the case for PCBM and aluminum, and results in the experimentally observed open circuit voltage dependence on the LUMO of PCBM [89].

The end result of the integer charge-transfer model is the so-called “Mark of Zorro” effect for a varying electrode work function, as illustrated in Figure 7 B). Under this model, the bulk heterojunction solar cell therefore has a maximum open circuit voltage dictated the difference between the E_{ICT+} state of the HOMO and the E_{ICT-} state of the LUMO.

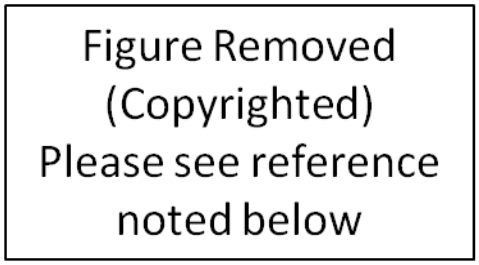

Figure 7 - A) Illustration of the integer charge-transfer model for organic-electrode interfaces. i) and iii) show Fermi level pinning of the electrode (denoted as 'sub' for substrate here) to the E_{ICT+} and E_{ICT-} states respectively. ii) shows "vacuum level alignment," which occurs when $E_{ICT-} < \phi_{electrode} < E_{ICT+}$ or tunnelling is energetically unfavourable. B) Variation in the 'observed' electrode work function for an organic/electrode interface as a function of the isolated work function of the pure electrode, as detailed by the integer charge-transfer model. C) Variation in the position of the integer charge-transfer states due to the image potential at the organic-electrode interface. (Images and figures adapted from ref [41])

It is now worth briefly noting the effects of injection materials placed between active organic materials and the electrodes. The use of LiF in between the organic layer and an aluminum top electrode has proven to be successful in improving both device efficiencies and increasing the solar cell open circuit voltage [53, 92]. It has been proposed that the thin LiF layer may lead to the formation of a dipole due to the preferential alignment of Li^+ to the organic surface and the F^- to the metal surface. This additional dipole would cause a down-shift in the vacuum level, opposing the vacuum level up-shift due to the integer charge-transfer model. Since the overall interfacial dipole is weaker, the aluminum Fermi level is pinned at some point above E_{ICT-}, resulting in an improved open circuit voltage. As a point of note, this understanding has been shown to be true for thick films of LiF; however, in monolayer films of LiF, LiF dissociation and doping effects are the likely cause for device improvement [93].

4. Solar Cell Circuit Model and Methods for Solar Cell Parameter Extraction

In all organic solar cell research, it is assumed that researchers use similar methods to obtain relevant solar cell parameters from the solar cell output IV characteristics. The equivalent circuit for a generic solar cell is shown in Figure 1, and is noted to have the following current-voltage relationship:

$$I_{total} = I = -I_{photocurrent} + I_{diode} + I_{shunt} \quad (4)$$

$$I = -I_{ph} + I_0\left(\exp\left[\frac{V+IR_s}{nV_{th}}\right] - 1\right) + G_{sh}(V + IR_s) \quad (5)$$

, where I_0 is the reverse saturation current, n is the diode ideality factor, $V_{th}=k_BT/q$ is the thermal voltage, R_s is the series resistance and G_{sh} is the shunt conductance ($G_{sh}=1/R_{sh}$).

It is important to note that the diode parameters in the equation above do not have the same explicit meanings as they do for single crystal p-n junction or Schottky junction diodes. However, these values are inherently related to equivalent processes that produce similar device behaviour in the organic devices. For example, since the diode ideality factor is strongly related to recombination in silicon p-n junctions, either by space charge recombination or high level injection, it is expected that this parameter is similarly related to recombination mechanisms in organic solar cells. As such, comparison of these parameters across different experimental organic solar cells can still yield important information regarding device operation.

The most frequently reported solar cell parameters are the open-circuit voltage, short-circuit current, fill factor and power conversion efficiency. These values are described in **Section 2** and are straightforward to calculate from solar cell output characteristics. However, the shunt and series resistances, which are arguably the next most useful parameters for organic solar cells, are not as simple to ascertain. In recent studies on organic solar cells, researchers used the slope of the output curve under dark conditions at V=0V and V=2V to find the shunt and series resistances respectively [63]. This very simple approach was described many years earlier for CdS thin film solar cells [94], and involves the assumption that the series resistance is small and the shunt resistance is large. This approach generally provides reasonable values for the shunt resistance based on the logic shown below:

- R_{shunt}: I_{ph}~=0 (dark output), so $I = I_0\left(\exp\left[\frac{V+IR_s}{nV_{th}}\right]-1\right)+G_{sh}(V+IR_s)$

  At the current axis V=0V, I is small and if R_s is small, $\exp\left[\frac{V+IR_s}{nV_{th}}\right] \cong \exp[0] = 1.$

  Further, G_{sh} is generally small because R_{sh} is ideally large, so $G_{sh}IR_s$ must be very small. We can therefore write, by means of simple logic:

$$I \cong I_0(1-1) + G_{sh}V + G_{sh}IR_s \cong G_{sh}V$$

$$I \cong G_{sh}V \; or \frac{dI}{dV} \cong G_{sh} \quad \therefore \frac{dV}{dI}(V=0V) \cong R_{sh}$$

However, as noted above, this method is only valid under the condition that the solar cell has reasonably good properties with a high R_{sh} and low R_s. Furthermore, the calculation for R_s is only valid if a 'good' voltage point is chosen for the slope calculation. In the study of organic solar cells, especially with new materials and varying solar cell architectures, the assumptions of low R_s and high R_{sh} are not strictly valid. In order to obtain more accurate values for both the series and shunt resistances as well as the diode parameters of the solar cell, one must fit the solar cell parameters to the current equation shown in (5) above.

There are numerous methods described in literature to extract the relevant diode parameters [95-99]. In this review, three of these methods are examined for their relative

success in analyzing sample IV output data representative of an illuminated organic solar cell. A summative comparison of the extracted parameters using several different methods is provided in Table 1. The MATLAB code for all methods examined in this review is provided in the **Supplemental Information,** attached at the end of this review.

The simplest manner to extract the solar cell parameters is through the use of a nonlinear least squared error fit where equation (5) is used to calculate current directly. Unfortunately, since equation (5) is a transcendental equation, it is difficult to solve for explicit current values. In order to circumvent this problem, it is convenient to use the Lambert W function, as described in greater detail in [99, 100]. After some algebra, equation (5) may be rearranged into the form:

$$I = -\frac{V}{R_s+R_{sh}} - \frac{nV_{th}}{R_s} \cdot LambertW\left[\frac{R_s I_0 R_{sh} e^{\left[\frac{R_{sh}\left(V+R_s I_0+R_s I_{ph}\right)}{nV_{th}(R_s+R_{sh})}\right]}}{nV_{th}(R_s+R_{sh})}\right] + \frac{R_{sh}(I_0+I_{ph})}{R_s+R_{sh}} \qquad (6)$$

, where LambertW is the Lambert W function and I_{ph} is assumed to be approximately equal to the short circuit current [99]. The results for this method are detailed under the heading 'Method 1' in Table 1 and Figure 8 below. Unfortunately, this method is computationally intensive and susceptible to divergence problems as well as local minima convergence issues. Furthermore, the requirement of initial guesses infers that the researcher has some knowledge regarding the device characteristics prior to analysis, which may not always be true.

As an alternative approach for efficient parameter extraction, Chegaar and coworkers developed a very simple, robust method for solving the solar cell parameters using only the illuminated-device IV characteristics of a solar cell [98]. This method is particularly appropriate for organic solar cells because it makes minimal assumptions regarding the device structure. This method also requires no prior knowledge regarding the solar cell parameters. Furthermore, it has been shown to work reasonably well with IV characteristics that contain a significant amount of noise.

In brief, Chegaar and coworkers modified equation (5) to collect the non-exponential current terms and then performed a shunt current correction to obtain I_c. The authors then re-wrote the current-voltage equation with the voltage as the dependent term and the current as the independent term, as shown below:

$$I_c = I_{pA} - I_0\left[exp\left(\frac{\beta}{n}(V+IR_s)\right)\right] \;\Rightarrow\; V = \frac{n}{\beta} ln\frac{I_{pA}}{I_0} + \frac{n}{\beta} ln\left(1-\frac{I_c}{I_{pA}}\right) - R_s I \qquad (7)$$

Since the right side of (7) is of the form $f(I) = C_0 + C_1 I + C_2 \ln\left(1-\frac{I_c}{I_{pA}}\right)$, it is simple to perform a simple least squares method to determine the relevant solar cell parameters. In this

particular study, the least squares approach is accomplished through the solution of a system of equations. This method, denoted 'Method 2,' proved to be very quick and yielded experimentally accurate and relevant data, as shown in Table 1 and Figure 8.

The final method examined in this review is based off of recent work by Nehaoua et. al. that was aimed to help with parameter determination for organic solar cells [96]. This method uses a very unique approach to solve for the series resistance and diode ideality factor, which involves linear regression on a set of data derived from subsets of the initial IV output data. The reader is encouraged to examine references [96, 101] for a more detailed explanation of this process. Unfortunately, this method proved to be rather unstable for the sample data examined in this review. The extracted diode parameters were found to vary strongly depending on the amount and range of input IV data passed to the MATLAB function. Regardless, the results are also presented as 'Method 3' in Table 1 and Figure 8.

Table 1 - Summary of Extracted Diode Parameters for Different Methods of Analysis on Sample Illuminated IV Organic Solar Cell Data

	I_{SC} (A)	V_{OC} (V)	FF	R_{sh} (Ω)	R_s (Ω)	n	I_0 (A)
Method 1, [99]	0.0064	0.6	0.4902	3.64E+04	38.2436	1.0688	2.21E-12
Method 2, [98]	0.0064	0.6	0.4902	3.63E+04	35.4685	1.3637	2.63E-10
Method 3, [96]	0.0064	0.6	0.4902	3.62E+04	107.4207	3.0274	2.00E-08*

**Method 3 does not provide a reverse saturation current. This value was determined graphically by attempting to best fit the model to the input data. It is noted that this simple approach may be an additional cause for error with this method.*

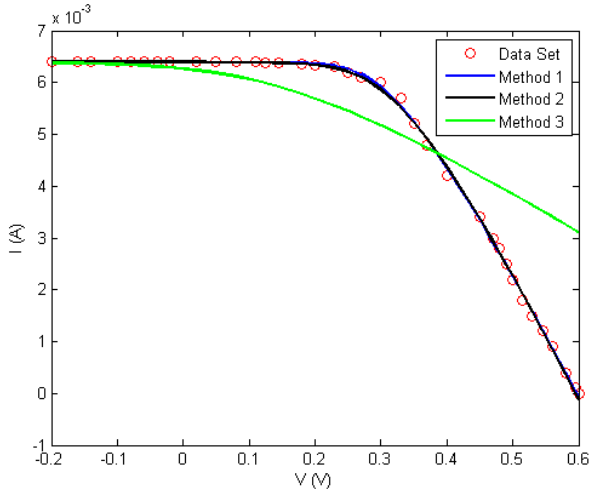

Figure 8 - Experimental and Modelled Solar Cell IV Output for Various Methods of Parameter Extraction

Method 3 did not converge to realistic or accurate solar cell parameters, in spite of what appear to be reasonable values in Table 1. It is feasible that the poor behaviour of this method is simply due to an error in its present implementation. Regardless the methods detailed by Jain and Kapoor in 2005 [99] and by Bouzidi et. al. in 2007 [98] have shown to provide very close fits to the illuminated IV data. From the tabulated data in Table 1, it is clear that variation between series and shunt resistances from both methods 1 and 2 are relatively small, indicating that cross comparisons between data using either method are valid. However, one should take precaution when cross-comparing diode ideality factors and reverse saturation current values, as they are shown to vary by up to ~1.3-times and 2 orders of magnitude respectively between the two methods for the same data set.

As an additional note, Schilinsky et. al. have examined a modified single-diode model where the photocurrent, I_{ph}, varies as a function of the applied voltage, such that the model can account for the field dependence of the photocurrent [102]. The authors note that a similar approach has been previously successful in the study of amorphous silicon diodes and solar cells. In typical models, the photocurrent is generally assumed to be equal to the short circuit current. In contrast, this model defines the photocurrent as shown below, which allows for accurate measurements over a wider range of illumination intensities.

$$I_{ph} = \begin{cases} -|I_{sc}| & \text{if } \mu\tau(-V + V_{bi})/L > L \\ |I_{sc}| & \text{if } \mu\tau(V - V_{bi})/L > L \\ |I_{sc}|\mu\tau(-V + V_{bi})/L^2 & else \end{cases}$$

This variation introduces the free carrier mobility, μ, the free carrier lifetime, τ, and the built in voltage of the junction as additional fitting parameters. While these fitting parameters should only be taken as estimates of their true values, they may provide crucial information in the study and comparison of organic solar cells among different research groups.

5. Conclusions: Achieving 10% Efficiency Solar Cells and Beyond

Organic solar cells have seen impressive gains in their device efficiencies over a very brief period, with most significant improvements achieved only within the past decade. This rapid progress is largely attributed to initial improvements in device architecture, followed by strong materials optimization through tailored polymeric donor materials. By shifting from a single layer solar cell to a planar heterojunction, researchers substantially decreased bimolecular recombination [18, 27, 28]. This development resulted in the realization of a donor-acceptor solar cell, which was inherently limited by exciton diffusion to the organic-organic interface. In order to address this limit, researchers then developed the bulk heterojunction to decrease the distance an exciton must travel before reaching an interface for dissociation into free carriers [37-39].

The subsequent realization of the P3HT:PCBM bulk heterojunction offered a basis for developing a stronger understanding for all organic and polymeric photovoltaics [55]. Most recent work has been dedicated to developing the basic chemistry to reliably fabricate high efficiency organic solar cells and to forming the physical models to adequately describe bulk heterojunction device behaviour. As one critical point, researchers have found that the efficiency of organic solar cells is very strongly controlled by the phase separation and molecular organization of the donor and acceptor materials. The intensive study of P3HT:PCBM solar cells has also highlighted a need for researchers to maintain both standard test conditions and standardized methodologies for solar cell parameter extraction and analysis.

With a better understanding of the organic solar cell fabrication chemistry and device physics, researchers now have a direct route to improving organic solar cell efficiency. The ability to custom tailor the HOMO and LUMO of polymers has allowed for the development of solar cells with specific device output properties in a very controlled manner. This has led to PTB7-PCBM solar cells with both high open circuit voltages and high short circuit currents, granting 7.40% power conversion efficiencies [86]. Furthermore, the development of the integer charge-transfer model provides strong insight into the origin of the open circuit voltage [41], which may allow for additional gains in device efficiency through optimization of organic-electrode interfaces.

With the groundwork for highly efficient bulk heterojunction organic solar cells established, researchers may now begin to examine less straightforward methods to enhance device efficiency. Such efforts include the development of solution-processable, polymeric tandem solar cells [103], which may prove to reduce thermalization losses. Researchers have also begun to use optical spacers to maximize the electric field of impingent light within the bulk of the active layer [83, 104]. The combination of this work with the optimization of both device materials and organic-electrode interfaces will ultimately lead to organic solar cells exceeding 10% efficiency.

Works Cited.

[1] P. Kamat, "Meeting the clean energy demand: Nanostructure architectures for solar energy conversion," *Journal of Physical Chemistry C,* vol. 111, pp. 2834–2860, 2007.

[2] M. Green*, et al.*, "Short Communication Solar cell efficiency tables (version 33)," *Progress in Photovoltaics: Research and Applications,* vol. 17, pp. 85-94, 2009.

[3] M. Green*, et al.*, "Very high efficiency silicon solar cells-science and technology," *Electron Devices, IEEE Transactions on,* vol. 46, pp. 1940-1947, 2002.

[4] W. Shockley and H. Queisser, "Detailed Balance Limit of Efficiency of p n Junction Solar Cells," *Journal of Applied Physics,* vol. 32, pp. 510-519, 1961.

[5] N. Gupta*, et al.*, "Prospects of Nanostructure-Based Solar Cells for Manufacturing Future Generations of Photovoltaic Modules," *International Journal of Photoenergy,* vol. 1, 2009.

[6] Solar Novus Today. (27 July 2010, Accessed: 9 November 2010). *Solarmer Energy, Inc. Breaks Psychological Barrier with 8.13% OPV Efficiency*. Available: http://www.solarnovus.com/index.php?option=com_content&view=article&id=1086:solarmer-energy-inc-breaks-psychological-barrier-with-813-opv-efficiency&catid=41:applications-tech-news&Itemid=245

[7] J. G. Xue*, et al.*, "Asymmetric tandem organic photovoltaic cells with hybrid planar-mixed molecular heterojunctions," *Applied Physics Letters,* vol. 85, pp. 5757-5759, Dec 2004.

[8] J. G. Xue*, et al.*, "4.2% efficient organic photovoltaic cells with low series resistances," *Applied Physics Letters,* vol. 84, pp. 3013-3015, Apr 2004.

[9] P. Peumans*, et al.*, "Small molecular weight organic thin-film photodetectors and solar cells," *Journal of Applied Physics,* vol. 93, p. 3693, 2003.

[10] M. Riede*, et al.*, "Small-molecule solar cells - status and perspectives," *Nanotechnology,* vol. 19, Oct 2008.

[11] H. Spanggaard and F. C. Krebs, "A brief history of the development of organic and polymeric photovoltaics," *Solar Energy Materials and Solar Cells,* vol. 83, pp. 125-146, Jun 2004.

[12] C. Tang and A. Albrecht, "Photovoltaic effects of metal–chlorophyll a–metal sandwich cells," *The Journal of Chemical Physics,* vol. 62, p. 2139, 1975.

[13] Y. Gao*, et al.*, "Interface formation of Ca with poly (p phenylene vinylene)," *Journal of Applied Physics,* vol. 73, pp. 7894-7899, 1993.

[14] H. Antoniadis*, et al.*, "Photovoltaic and Photoconductive Properties of Aluminum Poly(P-Phenylene Vinylene) Interfaces," *Synthetic Metals,* vol. 62, pp. 265-271, Feb 1994.

[15] W. Riess*, et al.*, "Electroluminescence and photovoltaic effect in PPV schottky diodes," *Journal of Luminescence,* vol. 60, pp. 906-911, 1994.

[16] R. Marks*, et al.*, "The photovoltaic response in poly (p-phenylene vinylene) thin-film devices," *Journal of Physics: Condensed Matter,* vol. 6, p. 1379, 1994.

[17] H. Hoppea and N. Sariciftci, "Organic solar cells: An overview," *J. Mater. Res,* vol. 19, p. 1925, 2004.

[18] C. Tang, "Two layer organic photovoltaic cell," *Applied Physics Letters,* vol. 48, pp. 183-185, 1986.

[19] V. I. Arkhipov*, et al.*, "Why is exciton dissociation so efficient at the interface between a conjugated polymer and an electron acceptor?," *Applied Physics Letters,* vol. 82, pp. 4605-4607, Jun 2003.

[20] S. A. Jenekhe and S. J. Yi, "Efficient photovoltaic cells from semiconducting polymer heterojunctions," *Applied Physics Letters,* vol. 77, pp. 2635-2637, Oct 2000.

[21] K. Tada*, et al.*, "Photocell with heterojunction of donor acceptor polymers," *Synthetic Metals,* vol. 102, pp. 982-983, Jun 1999.

[22] A. J. Breeze*, et al.*, "Polymer-perylene diimide heterojunction solar cells," *Applied Physics Letters,* vol. 81, pp. 3085-3087, Oct 2002.

[23] J. J. M. Halls and R. H. Friend, "The photovoltaic effect in a poly(p-phenylenevinylene)/perylene heterojunction," *Synthetic Metals,* vol. 85, pp. 1307-1308, Feb 1997.

[24] J. J. M. Halls*, et al.*, "Exciton diffusion and dissociation in a poly(p-phenylenevinylene)/C-60 heterojunction photovoltaic cell," *Applied Physics Letters,* vol. 68, pp. 3120-3122, May 1996.

[25] S. Morita*, et al.*, "Wavelength dependence of junction characteristics of poly (3-alkylthiophene)/C60 layer," *Japanese Journal of Applied Physics,* vol. 32, pp. L873-L874, 1993.

[26] L. S. Roman*, et al.*, "High quantum efficiency polythiophene/C-60 photodiodes," *Advanced Materials,* vol. 10, pp. 774-777, Jul 1998.

[27] N. Sariciftci*, et al.*, "Semiconducting polymer buckminsterfullerene heterojunctions: Diodes, photodiodes, and photovoltaic cells," *Applied Physics Letters,* vol. 62, pp. 585-587, 1993.

[28] N. Sariciftci*, et al.*, "Semiconducting polymers (as donors) and buckminsterfullerene (as acceptor): photoinduced electron transfer and heterojunction devices," *Synthetic Metals,* vol. 59, pp. 333-352, 1993.

[29] N. Sariciftci*, et al.*, "Photoinduced electron transfer from a conducting polymer to buckminsterfullerene," *Science,* vol. 258, pp. 1474-1476, 1992.

[30] S. Morita*, et al.*, "Doping Effect of Buckminsterfullerene in Conducting Polymer - Change of Absorption-Spectrum and Quenching of Luminescence," *Solid State Communications,* vol. 82, pp. 249-252, Apr 1992.

[31] C. Lee*, et al.*, "Sensitization of the photoconductivity of conducting polymers by C60: Photoinduced electron transfer," *Physical Review B,* vol. 48, pp. 15425-15433, 1993.

[32] M. Granstrom*, et al.*, "Laminated fabrication of polymeric photovoltaic diodes," *Nature,* vol. 395, pp. 257-260, Sep 1998.

[33] J. S. Huang*, et al.*, "A semi-transparent plastic solar cell fabricated by a lamination process," *Advanced Materials,* vol. 20, pp. 415-+, Feb 2008.

[34] H. Hoppe and N. Sariciftci, "Organic solar cells: An overview," *J. Mater. Res,* vol. 19, p. 1925, 2004.

[35] G. Yu*, et al.*, "Semiconducting polymer diodes: Large size, low cost photodetectors with excellent visible ultraviolet sensitivity," *Applied Physics Letters,* vol. 64, pp. 3422-3424, 1994.

[36] J. Hummelen, *et al.*, "Preparation and characterization of fulleroid and methanofullerene derivatives," *The Journal of Organic Chemistry,* vol. 60, pp. 532-538, 1995.
[37] G. Yu, *et al.*, "Polymer photovoltaic cells: enhanced efficiencies via a network of internal donor-acceptor heterojunctions," *Science,* vol. 270, p. 1789, 1995.
[38] G. Yu and A. Heeger, "Charge separation and photovoltaic conversion in polymer composites with internal donor/acceptor heterojunctions," *Journal of Applied Physics,* vol. 78, pp. 4510-4515, 1995.
[39] J. J. M. Halls, *et al.*, "Efficient Photodiodes from Interpenetrating Polymer Networks," *Nature,* vol. 376, pp. 498-500, Aug 1995.
[40] A. Crispin, *et al.*, "Transition between energy level alignment regimes at a low band gap polymer-electrode interfaces," *Applied Physics Letters,* vol. 89, Nov 2006.
[41] S. Braun, *et al.*, "Energy-Level Alignment at Organic/Metal and Organic/Organic Interfaces," *Advanced Materials,* vol. 21, pp. 1450-1472, Apr 2009.
[42] S. Sun, "Design of a block copolymer solar cell," *Solar Energy Materials and Solar Cells,* vol. 79, pp. 257-264, 2003.
[43] F. C. Krebs and M. Jorgensen, "Conducting block copolymers. Towards a polymer pn-junction," *Polymer Bulletin,* vol. 50, pp. 359-366, Jul 2003.
[44] U. Stalmach, *et al.*, "Semiconducting diblock copolymers synthesized by means of controlled radical polymerization techniques," *Journal of the American Chemical Society,* vol. 122, pp. 5464-5472, Jun 2000.
[45] B. de Boer, *et al.*, "Supramolecular self-assembly and opto-electronic properties of semiconducting block copolymers," *Polymer,* vol. 42, pp. 9097-9109, Oct 2001.
[46] Q. Zhang, *et al.*, "Donor- Acceptor Poly (thiophene-block-perylene diimide) Copolymers: Synthesis and Solar Cell Fabrication," *Macromolecules,* vol. 42, pp. 1079-1082, 2009.
[47] S. E. Shaheen, *et al.*, "2.5% efficient organic plastic solar cells," *Applied Physics Letters,* vol. 78, pp. 841-843, Feb 2001.
[48] S. Günes, *et al.*, "Conjugated polymer-based organic solar cells," *Chem. Rev,* vol. 107, pp. 1324-1338, 2007.
[49] C. Melzer, *et al.*, "Hole transport in poly(phenylene vinylene)/methanofullerene bulk-heterojunction solar cells," *Advanced Functional Materials,* vol. 14, pp. 865-870, Sep 2004.
[50] V. D. Mihailetchi, *et al.*, "Compositional dependence of the performance of poly(p-phenylene vinylene): Methanofullerene bulk-heterojunction solar cells," *Advanced Functional Materials,* vol. 15, pp. 795-801, May 2005.
[51] J. Kroon, *et al.*, "Accurate efficiency determination and stability studies of conjugated polymer/fullerene solar cells," *Thin Solid Films,* vol. 403, pp. 223-228, 2002.
[52] T. Munters, *et al.*, "A comparison between state-of-the-art 'gilch' and 'sulphinyl' synthesised MDMO-PPV/PCBM bulk hetero-junction solar cells," *Thin Solid Films,* vol. 403, pp. 247-251, Feb 2002.
[53] C. J. Brabec, *et al.*, "Effect of LiF/metal electrodes on the performance of plastic solar cells," *Applied Physics Letters,* vol. 80, pp. 1288-1290, Feb 2002.
[54] E. Bundgaard and F. C. Krebs, "Low band gap polymers for organic photovoltaics," *Solar Energy Materials and Solar Cells,* vol. 91, pp. 954-985, Jul 2007.

[55] P. Schilinsky, *et al.*, "Recombination and loss analysis in polythiophene based bulk heterojunction photodetectors," *Applied Physics Letters,* vol. 81, pp. 3885-3887, Nov 2002.
[56] F. Padinger, *et al.*, "Effects of postproduction treatment on plastic solar cells," *Advanced Functional Materials,* vol. 13, pp. 85-88, 2003.
[57] G. Dennler, *et al.*, "Polymer-Fullerene Bulk-Heterojunction Solar Cells," *Advanced Materials,* vol. 21, pp. 1323-1338, Apr 2009.
[58] C. J. Brabec, *et al.*, "Polymer-Fullerene Bulk-Heterojunction Solar Cells," *Advanced Materials,* vol. 22, pp. 3839-3856, Sep 2010.
[59] D. Chirvase, *et al.*, "Influence of nanomorphology on the photovoltaic action of polymer–fullerene composites," *Nanotechnology,* vol. 15, p. 1317, 2004.
[60] I. Riedel and V. Dyakonov, "Influence of electronic transport properties of polymer-fullerene blends on the performance of bulk heterojunction photovoltaic devices," *Physica Status Solidi a-Applied Research,* vol. 201, pp. 1332-1341, May 2004.
[61] J. S. Huang, *et al.*, "Influence of composition and heat-treatment on the charge transport properties of poly(3-hexylthiophene) and 6,6 -phenyl C-61-butyric acid methyl ester blends," *Applied Physics Letters,* vol. 87, Sep 2005.
[62] Y. Kim, *et al.*, "Device annealing effect in organic solar cells with blends of regioregular poly(3-hexylthiophene) and soluble fullerene," *Applied Physics Letters,* vol. 86, Feb 2005.
[63] G. Li, *et al.*, "High-efficiency solution processable polymer photovoltaic cells by self-organization of polymer blends," *Nature Materials,* vol. 4, pp. 864-868, Nov 2005.
[64] G. Li, *et al.*, "Investigation of annealing effects and film thickness dependence of polymer solar cells based on poly(3-hexylthiophene)," *Journal of Applied Physics,* vol. 98, Aug 2005.
[65] W. L. Ma, *et al.*, "Thermally stable, efficient polymer solar cells with nanoscale control of the interpenetrating network morphology," *Advanced Functional Materials,* vol. 15, pp. 1617-1622, Oct 2005.
[66] M. Reyes-Reyes, *et al.*, "High-efficiency photovoltaic devices based on annealed poly(3-hexylthiophene) and 1-(3-methoxycarbonyl)-propyl-1-phenyl-(6,6)C-61 blends," *Applied Physics Letters,* vol. 87, Aug 2005.
[67] T. J. Savenije, *et al.*, "The effect of thermal treatment on the morphology and charge carrier dynamics in a polythiophene-fullerene bulk heterojunction," *Advanced Functional Materials,* vol. 15, pp. 1260-1266, Aug 2005.
[68] P. Schilinsky, *et al.*, "Influence of the molecular weight of poly(3-hexylthiophene) on the performance of bulk heterojunction solar cells," *Chemistry of Materials,* vol. 17, pp. 2175-2180, Apr 2005.
[69] X. N. Yang, *et al.*, "Nanoscale morphology of high-performance polymer solar cells," *Nano Letters,* vol. 5, pp. 579-583, Apr 2005.
[70] R. C. Hiorns, *et al.*, "High molecular weights, polydispersities, and annealing temperatures in the optimization of bulk-heterojunction photovoltaic cells based on poly(3-hexylthiophene) or poly(3-butylthiophene)," *Advanced Functional Materials,* vol. 16, pp. 2263-2273, Nov 2006.

[71] Y. Kim, *et al.*, "A strong regioregularity effect in self-organizing conjugated polymer films and high-efficiency polythiophene: fullerene solar cells," *Nature Materials,* vol. 5, pp. 197-203, Mar 2006.

[72] V. D. Mihailetchi, *et al.*, "Origin of the enhanced performance in poly(3-hexylthiophene): 6,6 -phenyl C-61-butyric acid methyl ester solar cells upon slow drying of the active layer," *Applied Physics Letters,* vol. 89, Jul 2006.

[73] G. Li, *et al.*, ""Solvent annealing" effect in polymer solar cells based on poly(3-hexylthiophene) and methanofullerenes," *Advanced Functional Materials,* vol. 17, pp. 1636-1644, Jul 2007.

[74] W. Ma, *et al.*, "Effect of the molecular weight of poly(3-hexylthiophene) on the morphology and performance of polymer bulk heterojunction solar cells," *Macromolecular Rapid Communications,* vol. 28, pp. 1776-1780, Sep 2007.

[75] A. J. Moule and K. Meerholz, "Controlling morphology in polymer-fullerene mixtures," *Advanced Materials,* vol. 20, pp. 240-+, Jan 2008.

[76] M. Svensson, *et al.*, "High-performance polymer solar cells of an alternating polyfluorene copolymer and a fullerene derivative," *Advanced Materials,* vol. 15, pp. 988-+, Jun 2003.

[77] F. L. Zhang, *et al.*, "Influence of solvent mixing on the morphology and performance of solar cells based on polyfluorene copolymer/fullerene blends," *Advanced Functional Materials,* vol. 16, pp. 667-674, Mar 2006.

[78] L. H. Slooff, *et al.*, "Determining the internal quantum efficiency of highly efficient polymer solar cells through optical modeling," *Applied Physics Letters,* vol. 90, Apr 2007.

[79] E. G. Wang, *et al.*, "High-performance polymer heterojunction solar cells of a polysilafluorene derivative," *Applied Physics Letters,* vol. 92, Jan 2008.

[80] M. H. Chen, *et al.*, "Efficient Polymer Solar Cells with Thin Active Layers Based on Alternating Polyfluorene Copolymer/Fullerene Bulk Heterojunctions," *Advanced Materials,* vol. 21, pp. 4238-+, Nov 2009.

[81] N. Blouin, *et al.*, "A low-bandgap poly(2,7-carbazole) derivative for use in high-performance solar cells," *Advanced Materials,* vol. 19, pp. 2295-+, Sep 2007.

[82] N. Blouin, *et al.*, "Toward a rational design of poly(2,7-carbazole) derivatives for solar cells," *Journal of the American Chemical Society,* vol. 130, pp. 732-742, Jan 2008.

[83] S. H. Park, *et al.*, "Bulk heterojunction solar cells with internal quantum efficiency approaching 100%," *Nature Photonics,* vol. 3, pp. 297-U5, May 2009.

[84] Y. Y. Liang, *et al.*, "Highly Efficient Solar Cell Polymers Developed via Fine-Tuning of Structural and Electronic Properties," *Journal of the American Chemical Society,* vol. 131, pp. 7792-7799, Jun 2009.

[85] Y. Y. Liang, *et al.*, "Development of New Semiconducting Polymers for High Performance Solar Cells," *Journal of the American Chemical Society,* vol. 131, pp. 56-+, Jan 2009.

[86] Y. Liang, *et al.*, "For the bright future—bulk heterojunction polymer solar cells with power conversion efficiency of 7.4%," *Advanced Materials,* vol. 22, pp. E135-E138, 2010.

[87] J. Guo, *et al.*, "Structure, Dynamics, and Power Conversion Efficiency Correlations in a New Low Bandgap Polymer: PCBM Solar Cell," *The Journal of Physical Chemistry B,* vol. 114, pp. 742-748, 2009.

[88] A. Cravino, "Origin of the open circuit voltage of donor-acceptor solar cells: Do polaronic energy levels play a role?," *Applied Physics Letters,* vol. 91, Dec 2007.
[89] C. J. Brabec*, et al.*, "Origin of the open circuit voltage of plastic solar cells," *Advanced Functional Materials,* vol. 11, pp. 374-380, Oct 2001.
[90] M. Scharber*, et al.*, "Design Rules for Donors in Bulk Heterojunction Solar Cells—Towards 10% Energy Conversion Efficiency," *Advanced Materials,* vol. 18, pp. 789-794, 2006.
[91] B. Rand*, et al.*, "Offset energies at organic semiconductor heterojunctions and their influence on the open-circuit voltage of thin-film solar cells," *Physical Review B,* vol. 75, p. 115327, 2007.
[92] S. Shaheen*, et al.*, "Effects of inserting highly polar salts between the cathode and active layer of bulk heterojunction photovoltaic devices," in *Materials Research Society Symposium*, San Francisco, California, 2001, pp. 219-226.
[93] S. Jonsson*, et al.*, "Photoelectron spectroscopy of the contact between the cathode and the active layers in plastic solar cells: the role of LiF," *Japanese Journal of Applied Physics Part 1: Regular Papers, Short Notes and Review Papers,* vol. 44, p. 3695, 2005.
[94] F. Shirland, "The history, design, fabrication and performance of CdS thin film solar cells," *Advanced Energy Conversion,* vol. 6, pp. 201-202, 1966.
[95] Z. Ouennoughi and M. Chegaar, "A simpler method for extracting solar cell parameters using the conductance method," *Solid-State Electronics,* vol. 43, pp. 1985-1988, 1999.
[96] N. Nehaoua*, et al.*, "Determination of organic solar cell parameters based on single or multiple pin structures," *Vacuum,* vol. 84, pp. 326-329, 2009.
[97] M. Chegaar*, et al.*, "Simple parameter extraction method for illuminated solar cells," *Solid-State Electronics,* vol. 50, pp. 1234-1237, 2006.
[98] K. Bouzidi*, et al.*, "Solar cells parameters evaluation considering the series and shunt resistance," *Solar Energy Materials and Solar Cells,* vol. 91, pp. 1647-1651, 2007.
[99] A. Jain and A. Kapoor, "A new method to determine the diode ideality factor of real solar cell using Lambert W-function," *Solar Energy Materials and Solar Cells,* vol. 85, pp. 391-396, 2005.
[100] A. Jain and A. Kapoor, "A new approach to study organic solar cell using Lambert W-function," *Solar Energy Materials and Solar Cells,* vol. 86, pp. 197-205, 2005.
[101] A. Kaminski*, et al.*, "Non ideal dark IV curves behavior of silicon solar cells," *Solar Energy Materials and Solar Cells,* vol. 51, pp. 221-231, 1998.
[102] P. Schilinsky*, et al.*, "Simulation of light intensity dependent current characteristics of polymer solar cells," *Journal of Applied Physics,* vol. 95, pp. 2816-2819, Mar 2004.
[103] J. Kim*, et al.*, "Efficient tandem polymer solar cells fabricated by all-solution processing," *Science,* vol. 317, p. 222, 2007.
[104] J. Y. Kim*, et al.*, "New architecture for high-efficiency polymer photovoltaic cells using solution-based titanium oxide as an optical spacer," *Advanced Materials,* vol. 18, pp. 572-+, Mar 2006.

Supplemental Information

The MATLAB code used in the solar cell parameter extraction, as detailed in **Section 4**, is copied below. If the reader would like a copy of the ".m" function files or the data set used in this analysis, he or she may contact Graeme Williams at g3willia@uwaterloo.ca.

Method 1

Jain2005.m

```
function [  ] = Jain2005(IVData)
%This function calculates all of the relevant solar cell parameters given
%an input matrix IVData containing data in the form [Voltage Current]

%This script uses a very simple sum of squared approach to converge toward
%the ideal fitting parameters.  This script requires initial guess values.

%Constants
q = 1.602*10^-19;
k = 1.38*10^-23;
T = 298;
beta = q./(k.*T);
Vth = 1./beta;

global I V Isc Rsh

%-------------------------------------------------------------------------
%Breaking apart input matrix
V=IVData(:,1);
I=IVData(:,2);

%Finding the Isc (foo is a dummy variable)
[foo, SCindex] = min(abs(V));
Isc = I(SCindex);

%Finding the Voc
[foo, OCindex] = min(abs(I));
Voc = V(OCindex);

%Selecting the region of interest for the input data
V=IVData(SCindex+6:OCindex-1,1);
I=IVData(SCindex+6:OCindex-1,2);

%Using the slope at V=0V as Rsh (otherwise the function is under-defined and
%diverges)
Vlin=IVData(1:SCindex+1,1);
Ilin=IVData(1:SCindex+1,2);
[f,err] = polyfit(Vlin, Ilin,1);
Gsh = -f(1); %Defining the shunt resistance as the slope
Rsh = 1./Gsh;

%Initial guess values
Rs = 10;
n = 2;
I0 = 1*10^-10;

a= [Rs; n; I0];

%Calculating the modelling variables by minimizing SSE (using a
%user-defined function that takes the input data + initial guesses and
```

```
%outputs the sum of squared error)
solved = fminsearch(@diode_minerr, a);

%----------------------------------
%Fill factor and power calculations
V=IVData(:,1);
I=IVData(:,2);
Vmod = V(SCindex:OCindex);
Imod = I(SCindex:OCindex);

P = Vmod.*Imod;
[Pmax,Pmaxpt] = max(abs(P));
Vprime = Vmod(Pmaxpt);
Iprime = Imod(Pmaxpt);

FF = (Iprime.*Vprime)./(Voc.*Isc);
%----------------------------------

%Outputting relevant data
Isc
Voc
FF
Rsh
Rs = solved(1)
n = solved(2)
I0 = solved(3)
```

diode_minerr.m

```
function SSE = diode_minerr(a)
%This function requires the (global) data from the IV characteristics and
%the initial guesses for the fitting parameters.  It calculates the
%error between the diode-Rs-Rsh model and the experimental IV values.

%The rearranged, explicitly solved current equation (making use of the
%Lambert W function) was taken from Jain & Kapoor, 2005, "A new method to
%determine the diode ideality factor of real solar cell using Lambert
%W-function"

%Variables
q = 1.602*10^-19;
k = 1.38*10^-23;
T = 298;
beta = q./(k.*T);
Vth = 1./beta;

global I V Isc Rsh

%Exploding the a variable
Rs = a(1);
n = a(2);
I0 = a(3);

%Prediction of the current using the Lambert W function
Ipred = -V./(Rs+Rsh)-
lambertw(((Rs.*I0.*Rsh).*exp((Rsh.*(Rs.*Isc+Rs.*I0+V))./(n.*Vth.*(Rs+Rsh)))))./(Rs.*n.*
Vth+Rsh.*n.*Vth)).*(n.*Vth)./Rs + Rsh.*(I0+Isc)./(Rs+Rsh);

%Calculating sum of square errors
SSE = sum((Ipred-I).^2);
```

Method 2

Chegaar2007.m

```
function [  ] = Chegaar2007( IVData )
%This function calculates all of the relevant solar cell parameters given
%an input matrix IVData containing data in the form [Voltage Current]

%The methods of this script are based on the paper 'Ouennoughi and
%Chegaar,' 1999 - "A simpler method for extracting solar cell parameters
%using the conductance method"

%Variables
q = 1.602*10^-19;
k = 1.38*10^-23;
T = 298;
beta = q./(k.*T);


%-------------------------------------------------------------------------
%Breaking apart input matrix
V=IVData(:,1);
I=IVData(:,2);

%Finding the Isc (foo is a dummy variable)
[foo, SCindex] = min(abs(V));
Isc = I(SCindex);

%Finding the Voc
[foo, OCindex] = min(abs(I));
Voc = V(OCindex);

%Selecting the region of interest for the input data
V=IVData(SCindex+6:OCindex-1,1);
I=IVData(SCindex+6:OCindex-1,2);

%Calculating low bias correction values
Vlin=IVData(1:SCindex+1,1);
Ilin=IVData(1:SCindex+1,2);

%Computing the linear fit
[f,err] = polyfit(Vlin, Ilin,1);
%Defining the modified shunt resistance as the slope
Ga = -f(1);
Ipa = f(2);

%Calculating the corrected current
Ic = I - Ga.*V;

%-----
%Defining the variables of the least squares matrix
ls1 = sum(I.^2);

ls2 = 0;
for i = 1:length(I)
    ls2 = ls2 + I(i).*log(1-Ic(i)./Ipa);
end

ls3 = sum(I);

ls4 = sum(I);
```

```
ls5 = 0;
for i = 1:length(I)
    ls5 = ls5 + log(1-Ic(i)./Ipa);
end

ls6 = length(I);

ls7 = 0;
for i = 1:length(I)
    ls7 = ls7 + I(i).*log(1-Ic(i)./Ipa);
end

ls8 = 0;
for i = 1:length(I)
    ls8 = ls8 + (log(1-Ic(i)./Ipa)).^2;
end


ls9 = 0;
for i = 1:length(I)
    ls9 = ls9 + log(1-Ic(i)./Ipa);
end

lsmatrix = [ls1 ls2 ls3; ls4 ls5 ls6; ls7 ls8 ls9];
%------

a1 = sum(I.*V);

a2 = sum(V);

a3 = 0;
for i = 1:length(I)
    a3 = a3 + V(i).*log(1-Ic(i)./Ipa);
end

amatrix = [a1; a2; a3];

%Solving for the variables of the least squares matrix
C = linsolve(lsmatrix,amatrix);

%Solving for various parameters
Rs = -C(1);  %series resistance
n = beta.*C(2);  %diode ideality coefficient
I0 = Ipa.*exp(-C(3)./C(2));  %I0

foo = 1 - Ga.*Rs;  %dummy variable

Gsh = Ga./foo;  %shunt conductance
Rsh = 1./Gsh; %shunt resistance
Iph = Ipa./foo;   %photocurrent
Is = I0./foo;  %saturation current

%----------------------------------
%Fill factor and power calculations
V=IVData(:,1);
I=IVData(:,2);
Vmod = V(SCindex:OCindex);
Imod = I(SCindex:OCindex);

P = Vmod.*Imod;
[Pmax,Pmaxpt] = max(abs(P));
Vprime = Vmod(Pmaxpt);
Iprime = Imod(Pmaxpt);
```

```
FF = (Iprime.*Vprime)./(Voc.*Isc);
%---------------------------------

%Outputting relevant data
Isc
Voc
FF
Rsh
Rs
n
I0
```

Method 3

Nehaoua2010.m

```
function [  ] = Nehaoua2010( IVData )
%This function calculates Rs, Rsh and n given an input matrix IVData
%containing data in the form [Voltage Current]

%The method for parameter extraction is based on Nehaoua et. al. in
%'Determination of organic solar cell parameters based on single or
%multiple pin structures,' Vacuum, 2010.

%Reverse saturation current is not calculated in this particular method as
%the authors calculate I0 separately

%Variables
q = 1.602*10^-19;
k = 1.38*10^-23;
T = 298;
beta = q./(k.*T);

%-------------------------------------------------------------------------
%Breaking apart input matrix
V = IVData(:,1);
I = -IVData(:,2);

%Finding the location of Isc/Voc (foo is a dummy variable)
[foo, SCindex] = min(abs(V)); %min(abs(V))=y-axis intercept
Isc = I(SCindex);
[foo, OCindex] = min(abs(I)); %min(abs(I))=x-axis intercept
Voc = V(OCindex);

%Calculating the shunt conductance/resistance
Vlin = IVData(1:SCindex+6,1);
Ilin = -IVData(1:SCindex+6,2);
[f,err]=polyfit(Vlin, Ilin,1);
Gshunt=f(1); %This sets the conductance as the slope
Rsh = 1./Gshunt;

%Calculating shunt current
Ip = Gshunt.*V;
%Calculating the true current across the solar cell
I = I+Ip;

%Finding the new Isc & Voc taking shunt current into consideration
[foo, SCindex] = min(abs(V));
```

```
Isc = I(SCindex);
[foo, OCindex] = min(abs(I));
Voc = V(OCindex);

%Fill factor and power calculations
Vmod = V(SCindex:OCindex);
Imod = I(SCindex:OCindex);

P = Vmod.*Imod;
[Pmax,Pmaxpt] = max(abs(P));

Vprime = Vmod(Pmaxpt);
Iprime = Imod(Pmaxpt);

FF = (Iprime.*Vprime)./(Voc.*Isc);



%----------------------------------
%Rshunt, Rseries and n
%Redefining the range of data - only focusing on the region of 'diode'
%behaviour
V = IVData(1:OCindex-1,1);
I = -IVData(1:OCindex-1,2);
%Calculating shunt current
Ip = Gshunt.*V;
%Calculating the current across the solar cell
I = I+Ip;

%Solving for the linear regression parameters
X = [];
Y = [];
Iph = Isc; %Ishort circuit approximately equals photocurrent

for i = 1:(length(V)-1)
    for j = (i+1):length(V)
        if abs(Iph) > abs(I(j))  %Protection from noise, which can cause |I| > |Isc|
            if abs(Iph) > abs(I(i))  %Same as above
                X = [X; (V(j)-V(i))./(I(j)-I(i))];
                Y = [Y; (1./(I(j)-I(i))).*log((Iph-I(j))./(Iph-I(i)))];
            end
        end
    end
end

%Computing the linear fit
[f,err] = polyfit(X,Y,1);

%Solving for pertinent data
slope = f(1);
yint = f(2);
nval = beta./slope;
Rs = nval.*yint./beta;

%Outputting the relevant data
Isc
Voc
FF
Rsh
Rs
nval
```

Plotting Function

Plotting.m

```
function [  ] = Plotting( IVData, SolvedParam )

%Variables
q = 1.602*10^-19;
k = 1.38*10^-23;
T = 298;
beta = q./(k.*T);
Vth = 1./beta;

%Breaking apart input matrix
V=IVData(:,1);
I=IVData(:,2);

%Generic Solved Data
Isc = SolvedParam(1,1);
Voc = SolvedParam(1,2);
FF = SolvedParam(1,3);

%Method-specific Data
%Method 1
m1_Rsh = SolvedParam(1,4);
m1_Rs = SolvedParam(1,5);
m1_n = SolvedParam(1,6);
m1_I0 = SolvedParam(1,7);

%Method 2
m2_Rsh = SolvedParam(2,4);
m2_Rs = SolvedParam(2,5);
m2_n = SolvedParam(2,6);
m2_I0 = SolvedParam(2,7);

%Method 3
m3_Rsh = SolvedParam(3,4);
m3_Rs = SolvedParam(3,5);
m3_n = SolvedParam(3,6);
m3_I0 = SolvedParam(3,7);

%Creating a separate folder in which to save the figures
mkdir('DataFigures');
figsavepath = ['DataFigures\'];

%Model 1
Rsh = m1_Rsh;
Rs = m1_Rs;
n = m1_n;
I0 = m1_I0;
%Generating the model data
Ipred1 = -V./(Rs+Rsh)-
lambertw(((Rs.*I0.*Rsh).*exp((Rsh.*(Rs.*Isc+Rs.*I0+V))./(n.*Vth.*(Rs+Rsh)))).*(Rs.*n.*
Vth+Rsh.*n.*Vth)).*(n.*Vth)./Rs + Rsh.*(I0+Isc)./(Rs+Rsh);

%Model 2
Rsh = m2_Rsh;
Rs = m2_Rs;
n = m2_n;
I0 = m2_I0;
%Generating the model data
```

```
Ipred2 = -V./(Rs+Rsh)-
lambertw(((Rs.*I0.*Rsh).*exp((Rsh.*(Rs.*Isc+Rs.*I0+V))./(n.*Vth.*(Rs+Rsh)))).*(Rs.*n.*
Vth+Rsh.*n.*Vth)).*(n.*Vth)./Rs + Rsh.*(I0+Isc)./(Rs+Rsh);

%Model 3
Rsh = m3_Rsh;
Rs = m3_Rs;
n = m3_n;
I0 = m3_I0;
%Generating the model data
Ipred3 = -V./(Rs+Rsh)-
lambertw(((Rs.*I0.*Rsh).*exp((Rsh.*(Rs.*Isc+Rs.*I0+V))./(n.*Vth.*(Rs+Rsh)))).*(Rs.*n.*
Vth+Rsh.*n.*Vth)).*(n.*Vth)./Rs + Rsh.*(I0+Isc)./(Rs+Rsh);

%Creating a filename
figname = [figsavepath 'PlotComparison' '.png'];

figsave = figure;
p = plot(V,I,'o'); %Plotting experimental data
set(p,'Color','red')
hold on
q = plot(V,Ipred1,'-'); %Plotting Method 1
set(q,'Color','blue','LineWidth',2)
r = plot(V,Ipred2,'-'); %Plotting Method 2
set(r,'Color','black','LineWidth',2)
s = plot(V,Ipred3,'-'); %Plotting Method 3
set(s,'Color','green','LineWidth',2)
xlabel('V (V)');
ylabel('I (A)');
legend('Data Set', 'Method 1', 'Method 2', 'Method 3');
print(figsave, figname, '-dpng');

end
```